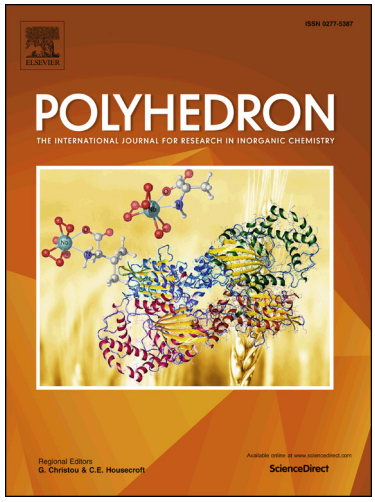

Synthesis, Electrochemistry and Electrocatalytic Activity of Cobalt Phthalocyanine Complexes - Effects of Substituents for Oxygen Reduction Reaction

Elif Turker Acar, Tuba Akkızlar Tabakoglu, Devrim Atilla, Fatma Yuksel, Gulten Atun

PII: S0277-5387(18)30335-8
DOI: https://doi.org/10.1016/j.poly.2018.06.018
Reference: POLY 13226

To appear in: *Polyhedron*

Received Date: 27 March 2018
Accepted Date: 5 June 2018

Please cite this article as: E.T. Acar, T.A. Tabakoglu, D. Atilla, F. Yuksel, G. Atun, Synthesis, Electrochemistry and Electrocatalytic Activity of Cobalt Phthalocyanine Complexes - Effects of Substituents for Oxygen Reduction Reaction, *Polyhedron* (2018), doi: https://doi.org/10.1016/j.poly.2018.06.018

Synthesis, Electrochemistry and Electrocatalytic Activity of Cobalt Phthalocyanine Complexes - Effects of Substituents for Oxygen Reduction Reaction

Elif Turker Acar[a*], Tuba Akkızlar Tabakoglu[b], Devrim Atilla[b], Fatma Yuksel[b], Gulten Atun[a]

[a]Istanbul University, Engineering Faculty, Department of Chemistry, TR-34320, Avcılar-Istanbul, TURKEY

[b]Gebze Technical University, Department of Chemistry, TR-41400, Gebze-Kocaeli, TURKEY.

*Corresponding author:

Dr. Elif TURKER ACAR

Phone: +902124737070

Fax: +902124737180

E-mail: elifacar@istanbul.edu.tr

eturkera@uci.edu

Abstract

The synthesis, characterization, electrochemistry and electrocatalytic activity of the mono (pyridine-4-oxy)- tri (tert-butyl) phthalocyaninato Co(II) (**Pc1**) and mono (pyridine-4-oxy)- hexa (hexyl) phthalocyaninato Co(II) (**Pc2**) are reported here. One reversible and one irreversible oxidation couples and two quasi-reversible reduction couples are observed for two complexes on the cyclic voltammograms. Both cobalt phthalocyanine derivatives (CoPcs) and multiwall carbon nanotube (MWCNT) composite (CoPcs/MWCNT) electrodes are coated on glassy carbon electrodes and used as electrocatalysts for oxygen reduction reaction (ORR). The morphology of composite surfaces is characterized using Scanning Electron Microscope (SEM). The results obtained using rotating disk electrode (RDE) reveal that the high catalytic activity is observed with $4e^-$ and mixed $2e^-$ - $4e^-$ ORR mechanisms for **Pc1/MWCNT** and **Pc2/MWCNT** hybrid catalysts in alkaline media, respectively. The tert-butyl substituent is more efficient with desired $4e^-$ mechanism on the catalytic activity of the composite electrode compared to the hexyl substituent on the CoPc ring.

Keywords: Cobalt Phthalocyanine, Substituent Group Effect, Electrocatalytic Activity, Oxygen Reduction Reaction, Multiwall Carbon Nanotube.

1. Introduction

The oxygen reduction reaction (ORR) is the most important reaction in life processes, and has attracted great interest in a variety of electrochemical technologies and applications including electrocatalysts, metal-air batteries [1], air-breathing cathodes [2] and especially energy converting systems such as fuel cells [3-4]. The efficiency of ORR electrocatalysts plays a crucial role in these applications.

Phthalocyanine (Pc) complexes have been comprehensively studied due to their important applications in many areas. These highly stable macrocyclic π-electronic systems exhibit many interesting features such as planarity and electronic delocalization, high symmetry, efficient light absorption and stability. Besides common usages as dyes and pigments, the Pc complexes have recently been considered as candidates for more advanced applications including data storage [5], solar energy conversion [6], photocatalysis [7], photonics [8], gas and radiation sensors [9], photodynamic therapy (PDT) [10] and fuel cells [11].

Phthalocyanines containing Co as the redox-active metal are also known to catalyze many important reactions. Co phthalocyanine (CoPc), which is a transition metal macrocycle, exhibits a unique ORR capability for alternative cathode catalysts [12], due to its large conjugated molecular structure with strong π-π interactions between aromatic rings. CoPc was reported as the first alternative cathode to noble metals [13]. However, the poor conductivity and instability of these metal phthalocyanine (MPc) catalysts necessitate the usage of conductive supports, which limit their employability in fuel cells [14-15]. Many reports have shown that MPc supported on carbon materials can greatly enhance the electrocatalytic

performance for ORR. The structure and the morphology of the electrode materials strongly affect the electrochemical properties in terms of their possible applications and performances.

As a new member of the carbon derivatives [16], carbon nanotubes (CNTs) have generated intense interest as catalyst supports in fuel cells because of their unique one-dimensional nanostructure, excellent chemical and thermal stability, high surface areas and thermal conductivity [17-18].

In recent years, CoPc catalysts supported on carbon derivatives have been studied as metal complex catalysts for oxygen electroreduction. In particular, CoPc compounds supported with multiwall carbon nanotubes (MWCNTs) have attracted great attention as potential catalysts for ORR in fuel cells due to the improved electrocatalytic activity of the assembly [19-21]. Planar CoPc absorbed on carbon black catalyzes O_2 reduction mainly through a four-electron process [22]. Two graphite (GR)-MPc nanocomposites, GR-CoPc and GR-FePc, were successfully supported on graphene oxide (GOx). GRCoPc/GOx modified electrodes showed a good electrocatalytic ability towards mediated oxidation of glucose, and GR-FePc composites exhibited excellent ORR activity at significantly less overpotential [23]. Co and Fe phthalocyanines and Co porphyrins were modified on different types of CNTs, single-wall (SWCNT), double-wall (DWCNT), and multi-wall (MWCNT), and their functionalized forms were effectively used for ORR applications. It has been found that the functionalized MWCNT is the most efficient catalysts for ORR applications [19]. The possibility of using N-rich ligand complexes as new electrocatalysts has been investigated with different pyridine complexes supported on carbon-CoPc (CoPc/C). The results have shown that their ORR catalytic activities are significantly improved after modification [24].

Besides CNT support, the substituent groups of phthalocyanine also have a very important role in ORR activities. Modification of pyridine derivatives can improve the catalytic ORR activity of carbon supported CoPc [24-25]. For instance, graphene supported FePc containing tert-pyridine groups has high electrocatalytic performance and is an ideal candidate for the replacement of commercial Pt/C for ORR [26]. Oppositely, tert-butyl substitutions on iron phthalocyanines (FePc) decrease ORR activity compared to the unsubstituted compounds [27]. Tert-butyl substituted cobalt phthalocyanines could also serve as soluble OER catalysts to enhance charging performance for Li-O_2 batteries [28].

In this paper, we investigate the synthesis, characterization and electrochemical properties of the mono (pyridine-4-oxy)- tri (tert-butyl) phthalocyaninato Co(II) (Pc1) and mono (pyridine-4-oxy)- hexa (hexyl) phthalocyaninato Co(II) (Pc2) compounds. The ORR electrocatalytic activities of complexes supported by MWCNTs on the glassy carbon electrode (GCE) were compared with bare and complex modified GCE in alkaline and acidic media. The role of substituent groups on the ORR catalytic activity of CoPcs (**Pc1** and **Pc2**) and MWCNT-supported CoPcs (**Pc1/MWCNT** and **Pc2/MWCNT**) hybrid catalysts was evaluated using cyclic voltammetry (CV) and rotating disk electrode (RDE) techniques. The effectiveness of MWCNTs on ORR catalytic behaviors of CoPc are already known. Our work extends this by studying the effect of substituent groups on ORR activity of MWCNT/CoPc hybrid catalysts. CoPc complexes including both pyridyl and tert butyl, hexa-hexyl groups and their use as catalysts for the ORR are reported here for the first time. These results demonstrate that very high ORR activity occurs for tert-butyl containing CoPc when compared with hexa-hexyl containing CoPc in the same one-pyridyl substituted CoPc/MWCNTs. Contrary to what is known for FePc, CoPc including tert-butyl groups gives exceptional results on ORR activity and has much higher ORR activity than other CoPc complexes that have been studied.

2. Experimental Section

2.1. Materials

All solvents, chemicals and 1-*tert*-butyl-3,4-dicyanobenzene (**1**) used for synthesis were reagent-grade quality and obtained from commercial suppliers. Preparative thin layer chromatography was performed on silica gel 60 P F_{254}. Commercial grade multi wall nanotubes (MWCNTs > %95) were purchased from Sigma Aldrich. MWCNTs were functionalized by treatment in concentrated H_2SO_4:HNO_3 (3:1) mixture and stirred at 70^oC for 2 hours. The MWCNTs were then separated from the concentrated acid solution and washed with ultrapure water. Finally, the purified MWCNT were dried in the drying-oven at 70^oC for 12 hours [29]. Nafion® solution (0.5wt. % in alcohol), ethanol, HNO_3, H_2SO_4 and tetrahydrofuran (THF) were purchased from Sigma Aldrich and used as received. Ultrapure water (18.2 µS resistivity at room temperature) was used in all experiments.

2.2. Instrumentation

Elemental analysis was obtained using a Thermo Finnigan Flash 1112. Infrared spectra were recorded between 4000 and 650 cm^{-1} using a Perkin Elmer Spectrum 100 FT-IR spectrometer with an attenuated total reflection (ATR) accessory featuring a zinc selenide (ZnSe) crystal. The mass spectra were recorded via Electrospray Ionization (ESI), using a Bruker Micro TOF-ESI/MS spectrometer.

X-ray suitable single crystals of compound **2** were obtained by crystallization in ethanol in the freezer at approximately -20 °C. Intensity data were recorded on a Bruker APEX II QUAZAR diffractometer using Mo Kα x-radiation (λ=0.71073 Å). Absorption correction was performed by the multi-scan method implemented in SADABS [30] and space groups were determined using XPREP implemented in APEX2 [31]. Structures were determined using the direct

methods procedure in SHELXS-97 and refined by full-matrix least squares on F2 using SHELXL-97 [32]. All non-hydrogen atoms were refined with anisotropic displacement factors and C-H hydrogen atoms were placed in calculated positions and allowed to ride on the parent atom. The final geometrical calculations were carried out with PLATON [33] and MERCURY [34] programs and the molecular drawings were done with DIAMOND [35] program. The structure has been deposited to the Cambridge Crystallographic Data Centre with CCDC-863723 reference code.

Cyclic Voltammetry (CV) experiments were carried out on Ivium Vertex potentiostat/galvanostat system with a conventional three electrode cell. A GCE with 3.0 mm diameter was used as the working electrode. The circuit was completed with a saturated Ag/AgCl and a platinum wire, which served as the reference and counter electrode, respectively. Measurements were performed in $5x10^{-4}$M CoPc solutions containing 0.1 M of tetrabutylammonium perchlorate (TBAP) supporting electrolyte under a nitrogen atmosphere.

ORR experiments in acidic and alkaline medium were conducted a with Britton-Robinson buffers of pH 2.4 and 11.8, respectively [36]. ORR measurements were carried out using Gamry Instruments Reference 600 Potentiostat/Galvanostat ZRA system in combination with Gamry Instruments RDE 710 Rotating Disc Electrode (Gamry Instruments, Inc., Warminster, PA, USA) coupled with a conventional three-compartment electrochemical cell. Rotating GCE was used as the working electrode and other electrodes were the same as CV measurements. SEM images of the modified GCE electrodes were obtained using a Jeol-JSM 5600 scanning electron microscope. All electrochemical experiments were performed at room temperature (25 ± 2 ^{o}C).

2.3. Synthesis

The synthesis of 1,2-dihexyl-4,5-dibromobenzene (**2**) [37], 1,2-dihexyl-4,5-dicyanobenzene (**3**) [37], and 1-(pyridine-4-oxy) 3,4-dicyanobenzene (**4**) [38] were achieved according to published procedures (Scheme 1).

Here "Scheme 1"

5-(Pyridine-4-oxy)-*1H*-isoindole-1,3(*2H*)-diimine (5): Compound **5** was prepared from 1-(pyridine-4-oxy) 3,4-dicyanobenzene (**4**). NH_3 gas was slowly bubbled through a stirred mixture of compound **4** (0.05 mol), CH_3ONa (0.025 mol) and dry methanol (70 ml) for 1 h at room temperature. The mixture was refluxed for 7 h with continuous NH3 introduction. Then, the resultant mixture was cooled to room temperature, filtered, and washed with water, ethanol and diethyl ether. Finally, the yellow solid product was dried under vacuum. Yield: 9.16 g, 77%, IR ν_{max} (cm^{-1}) (ATR): 3281, 3255, 3100-2800, 1694, 1602, 1529, 1428. Micro TOF-ESI/MS (*m/z*) calcd for $C_{13}H_{10}N_4O$: 238.09, found: 261.21 $[M+Na]^+$.

Mono (pyridine-4-oxy)- tri (*tert*-butyl) phthalocyaninato Co(II) (Pc1): Pc1 was synthesized from the condensation of a mixture of the phthalonitrile derivatives **1** and **5**. A mixture of **1** (190.59 mg, 0.8 mmol), **5** (95.2 mg, 0.4 mmol), 0.4 mmol anhydrous $Co(AcO)_2$ and 3 ml dimethylaminoethanol (DMAE) were refluxed for 18 h under argon atmosphere. After cooling down to room temperature, the solvent was removed under vacuum. The dark blue crude product was purified by preparative thin layer chromatography (TLC) using 10:1 CH_2Cl_2/EtOH solvent system. The pure dark blue solid compound was isolated. Yield: 30 mg,

(10%); Anal. Calcd. for $C_{49}H_{43}CoN_9O$: C, 70.66; H, 5.20; N, 15.14 %; Found C, 70.49; H, 5.33; N, 14.90; IR ν_{max} (cm^{-1}) (ATR): 3064 (CH_{ar}), 2956, 2903 and 2866 (CH_{al}), 1635 (C=N), 1613, 1569, 1520, 1482,1459, 1407, 1321, 1256, 1188, 1091 (C-O),1056, 827,752; Micro TOF-ESI/MS (*m/z*) calcd for $C_{49}H_{43}CoN_9O$: 1168.07 found: 1168.25 $[M]^+$.

Mono (pyridine-4-oxy)- hexa (hexyl) phthalocyaninato Co(II) (Pc2): Pc2 was synthesized from the condensation of a mixture of the phthalonitrile derivatives **3** and **5**. A mixture of **3** (355.2 mg, 1.2 mmol), **5** (95.2 mg, 0.4 mmol), 0.4 mmol anhydrous $Co(AcO)_2$ and 3 ml dimethylaminoethanol (DMAE) were refluxed for 24h under argon atmosphere. After cooling down to room temperature, the solvent was removed under vacuum. The dark blue crude product was purified by preparative thin layer chromatography (TLC) using 20:1 CH_2Cl_2/EtOH solvent system. The pure dark blue solid compound was isolated. Yield: 75 mg, (16%); Anal. Calcd. for $C_{73}H_{91}CoN_9O$: C, 74.97; H, 7.84; N, 10.78 %; Found C, 74.45; H, 8.10; N, 10.40; IR ν_{max} (cm^{-1}) (ATR): 3064 (CH_{ar}), 2954 and 2854 (CH_{al}), 1637 (C=N), 1613, 1571, 1522, 1464, 1189, 1102 (C-O); Micro TOF-ESI/MS (*m/z*) calcd for $C_{73}H_{91}CoN_9O$: 1168.10 found: 1168.25 $[M]^+$.

2.4. Catalyst Preparation

A portion of functionalized MWCNT powder was added into CoPc solution in THF to give a 2/1 weight ratio of CoPc/MWCNT. The solution was ultrasonicated for 20 min to form a homogeneous dispersion. The CoPc/MWCNT hybrid catalyst powders were obtained after evaporation of the solvent under a nitrogen stream. The catalyst ink solutions were prepared by sonicating CoPc/MWCNT powders in 0.75 ml of ethanol and 75 µl of Nafion® solution (0.5 wt.% in alcohol) [19].

2.5. Electrode Preparation

The glassy carbon (GC) disk used as rotating electrode was polished with 0.1 mm alumina slurry (Buehler Micropolish) using polishing pad (Buehler-102 mm) and washed with water, then it was similarly polished with 0.05 mm alumina slurry and sonicated with water before each measurement. To create a smooth film, each active layer was deposited by dropping 10 µL onto the GC disk from as-prepared catalyst inks and drying under ambient environment. Before all measurements, the solutions were saturated with air for ten minutes by bubbling air.

3. Results and Discussion

3.1. Synthesis and Characterization of Complexes

Despite, 1,2-dihexyl-4,5-dibromobenzene (**2**) is an oily liquid in room temperature, single crystals of the compound were obtained by cooling to -20 ℃ in ethanol. Its molecular structure was established by x-ray diffraction at 120 (2) K. The selected data collection and refinement details were presented in Table 1 and the crystal structure was given in Figure 1. Compound **2** has a monoclinic crystal system, *C2/c* space group and molecule sit on symmetry centre [symmetry operation is (#): -x+2, y, -z+3/2].

Here "Table 1"

Here "Fig. 1"

Usually, the substituted Pcs are synthesized by cyclotetramerization reaction of substituted phthalonitrile or the more reactive 1,3-diimino-1*H*-isoindol derivatives. In this study, 1,3-diimino-1*H*-isoindol derivatives of **4** were used to increase the asymmetric Pc derivatives

because the reactivity of phthalonitrile derivative (**4**) was lower than the other phthalonitrile derivatives (**1** or **3**). The syntheses of the desired asymmetric compounds (**Pc1** and **Pc2**) were accomplished by the statistical condensation reaction of two different precursors, the phthalonitrile derivatives (**1** or **3**) and the 1,3-diimino-1*H*-isoindol derivative (**5**) as given in Scheme 1. The condensation reaction of these compounds was achieved in dried DMAE in the presence of anhydrous metal salt. The asymmetric Pc derivatives (**Pc1** and **Pc2**) were easily purified by preparative thin layer chromatography.

Elemental analysis results of new Pcs (**Pc1** and **Pc2**) were supported to the recommended formulations with theoretical and experimental data were close together and the results were given in the experimental section. The ATR-IR spectral results of the Pcs (**Pc1** and **Pc2**) proved the proposed structure. The sharp peak for the CαN vibrations around 2220-2240 cm^{-1} belonging to nitrile groups disappeared after conversion of the nitrile derivatives to the Pcs. In addition, the observation of a group of intense bands in the range of 2854-2954 cm^{-1} in ATR-IR spectra of both compounds can be attributed to the C-H stretching vibrations of alkyl chains. The mass spectra of these compounds were obtained by ESI/MS technique and the molecular ion peaks of both Pc compounds were observed.

3.2. Cyclic Voltammetry

Cyclic voltammograms (CVs) of Co phthalocyanine derivatives were used to estimate their electron transfer abilities and electrochemical mechanism in THF, which is an organic donor solvent [39]. The CVs of the complexes, **Pc1** and **Pc2**, were recorded in the potential range of (-1.8) - 1.5 V versus Ag/AgCl and presented in Fig. 2. Both complexes showed similar excellent voltammetric behavior including four redox processes in THF. One reversible and

one irreversible oxidative response were observed on the positive side and two quasi-reversible reductive couples appeared on the negative side of the CVs for both complexes.

Here "Fig. 2"

Fig. 3 (a-b) shows the CVs of **Pc1** and **Pc2** with different scan rates in 0.1 M TBAP/THF solution system. As shown in Fig. 3 (a-b), the peak intensity of both complexes increases regularly, and peak potentials do not change substantially with the scan rate. Peak current was found to have a square-root dependence on scan rate ($I_p/v^{1/2}$), as shown in Fig. 4. The electrochemical parameters obtained from CVs at the lowest and highest scan rates were also compared in Table 2. All electrode processes were characterized by the ratio of cathodic to anodic peak currents (I_{pc}/I_{pa}), peak-to-peak separation (ΔE_p) and the effect of the scan rate to the ΔE_p.

Here "Fig. 3"

For **Pc1**, negative potential scans showed two reductive couples at -0.38 V and -1.45 V formal potentials, and anodic scans showed two oxidative responses at 0.77 V and 1.07 V. Although the I_{pa}/I_{pc} ratios were around 1.0, the reduction processes **I** and **II** have a quasi-reversible character due to their ΔE_p values higher than 60 mV (Table 2) and can be attributed to Co(I)Pc(-2)/Co(I)Pc(-3) and Co(II)Pc(-2)/Co(I)Pc(-2), respectively.

Here "Table 2."

Process **III** can be assigned to metal center reversible oxidative Co(II)Pc(-2) / Co(III)Pc(-2) couple (ΔE_p between 60-80 mV and I_{pa}/I_{pc} about 1.0) and the ligand based second oxidation redox couple (**IV**), I_{pa}/I_{pc} about 2.55, shows an irreversible character attributed to the Co(III)Pc(-2) / Co(III)Pc(-1) versus Ag/AgCl with a ΔE_p of 130 mV at 0.050 V/s scan rate, in spite of the fact that it couples during the reverse scan [40]. A linear relation was observed between the peak current and the square root of scan rate for the redox process of (**I**, **II** and **III**). The ratio of I_{pc}/I_{pa} is approximately unity and has no change considerably with increasing scan rates. This phenomenon also shows the diffusion-controlled mass transfer of the process. However, for redox process **IV**, the nonlinearity of the $I_p/v^{1/2}$ line indicates the complication of the mass transfer mechanism with the previous chemical reaction (Fig. 4a).

Here "Fig. 4"

Although the substituent of **Pc2** is quite different, it shows similar voltammetric behavior to **Pc1.** The first couple at –0.39 V obtained during reductive scan for **Pc2** could be easily attributed to the Co(II)Pc(−2)/Co(I)Pc(–2) reduction process (**II**) and the first oxidative couple at 0.72 V, to the Co(II)Pc(–2)/Co(III)Pc(–2) oxidation process (**III**) in THF. The second oxidation process (**IV**) at 1.05 V could be assigned to the Co(III)Pc(–2)/Co(III)Pc(–1) process and second reduction process (**I**) Co (I)Pc(-2)/ Co (I)Pc(-3) at -1.44 V.

3.3. Morphological Characterization of Catalysts

The morphology of composite surfaces was characterized by using SEM. The SEM image of **Pc1** deposited on GCE shows a sponge like structure (Fig. 5a). Nafion® increases stability of the composites and also stabilizes the CoPc by compressing it around the nanotubes [41]. As

seen from the film surfaces in Fig. 5b and 5c, CoPcs/MWCNT composites bound together with Nafion® successfully deposited, exhibiting a special three-dimensional nanotube or nanofiber structure on GCE surface. After deposition of the Nafion/CoPc mixture on the MWCNTs, a homogeneous catalyst-polymer layer was formed on the GCE surface [41]. **Pc1/MWCNT** and **Pc2/MWCNT** composite electrodes had uniform capsule-like morphology and completely covered the GC surface [20].

Here "Fig. 5"

3.4. Electrocatalysis of Oxygen Reduction Reaction (ORR)

The catalytic effect of the **Pc1**, **Pc2**, **Pc1/MWCNT** and **Pc2/MWCNT** electrodes for ORR was investigated by cyclic and rotating disc voltammetry (RDV) techniques.

3.4.1. Electrocatalytic Activity in Alkaline Media

To investigate the catalytic efficiency of the novel phthalocyanines for the ORR, each compound (**Pc1** and **Pc2**) and their hybrid counterparts (**Pc1/MWCNT** and **Pc2/MWCNT**) with acid functionalized MWCNT were deposited on the GCE surface using the drop-casting method.

CVs which were recorded in air-saturated BR buffer solution of pH 11.8 showed cathodic peaks in the potential region between -0.8 and 0.5 V for each complex indicating the oxygen reduction process (Fig. 6). For all electrodes, ORR peak potentials and the corresponding current densities were compared to estimate the catalytic efficiency. The bare GC electrode without Pc coating showed a low ORR peak around -0.58 V in the same alkaline solution.

Here "Fig. 6"

The **Pc1** catalyst presented a more positive ORR peak potential (around -0.46 V) in alkaline media compared to **Pc2** catalyst (around -0.52 V). The complexes had anodic shifts of about 120 mV and 60 mV compared to the bare electrode illustrating good catalytic effect (Fig. 6 (a-b). The peaks for the oxygen reduction were observed to be -0.39 V and -0.42 V for the **Pc1/MWCNT** and **Pc2/MWCNT**, respectively. Although all modified electrodes showed a catalytic effect for ORR, the **Pc1/MWCNT** was considered as the most efficient catalysts due to having the highest current density. Thus, for two complexes containing one pyridine group, the tert-butyl substituted **Pc1** complex and hybrid catalyst (**Pc1/MWCNT**) exhibited a superior catalytic effect than the hexyl-substituted **Pc2** compound in alkaline BR buffer solution.

3.4.2. Electrocatalytic Activity in Acidic Media

No reduction process occurred for the complexes in acidic BR buffer solution (pH 2.4) under nitrogen atmosphere. Similarly, for the bare electrode, no ORR peak was observed in acidic solution. The plots for the GC electrodes coated with **Pc1** and **Pc2** complexes showed the oxygen reduction peaks at around -0.40 V and -0.43 V, respectively. At the same conditions, the broad ORR peaks were observed in both CV voltammograms at around -0.310 V and -0.330 V for **Pc1/MWCNT** and **Pc2/MWCNT**, respectively. The reduction peak of the **Pc2/MWCNT** hybrid catalysts shifted to more positive potentials with respect to **Pc2** at around 100 mV (Fig. 7).

Here "Fig. 7"

3.4.3. RDV Measurements

Electroreduction of oxygen in alkaline and acidic aqueous solutions can occur mainly via two different reaction pathways. In alkaline pH, this process can involve the 2 e^- reduction pathway to generate the hydrogen peroxide anion HO_2^- (eq 1) or a direct 4 e^- reduction pathway to generate hydroxide (OH^-) (eq 3). On the other hand, it can lead to the production of a stable hydrogen peroxide species (H_2O_2) (eq 4) or water (H_2O) (eq 5) in acidic pH. The H_2O_2 species can be reduced to H_2O in more negative potentials (eq 6). For the fuel cells, the 4e^- process is a desirable route due to an increase in the maximum energy storage capacity allowed.

$$O_2 + H_2O + 2e^- \rightarrow HO_2^- + OH^- \quad (1)$$

$$HO_2^- + H_2O + 2e^- \rightarrow 3OH^- \quad (2)$$

$$O_2 + 2H_2O + 4e^- \rightarrow 4OH^- \quad (3)$$

$$O_2 + 2H^+ + 2e^- \rightarrow H_2O_2 \quad (4)$$

$$H_2O_2 + 2H^+ + 2e^- \rightarrow 2H_2O \quad (5)$$

$$O_2 + 4H^+ + 4e^- \rightarrow 2H_2O \quad (6)$$

To calculate the number of electrons, the polarization curves and K–L plots for CoPcs and CoPcs/MWCNT hybrid catalysts were studied according to RDE measurements in air-saturated BR buffer solution (pH 11.8). As expected, the limiting current densities increased

as a function of the rotation rate in the hydrodynamic system. Fig. 8 (a-e) shows the RDE voltammograms for the uncoated GC disk electrode and its coated analogs with **Pc1, Pc1/MWCNT, Pc2, Pc2/MWCNT** at various rotation rates.

Here "Fig. 8"

The onset potential is independent of the rotation rate and remains constant for the same catalysts. The onset ORR potential on the **Pc1** and **Pc2** catalysts started at 160 mV and 270 mV vs. Ag/AgCl, respectively, and shifted considerably towards the negative potential compared to **Pc1/MWCNT** (86 mV) and **Pc2/MWCNT** (120 mV) hybrid catalysts.

RDE plots ($1/i_L$ vs. $1/\omega^{-1/2}$) were drawn according to Koutecky–Levich (K–L) equation (eq 7) described as:

$$i_L = 0{,}62nFAD^{2/3}C_0\upsilon^{-1/6}\omega^{1/2} \quad (7)$$

Herein i_L is the apparent current density, n is the number of electrons transferred in the half reaction, F is the Faraday constant (96500 $Cmol^{-1}$), D is the diffusion coefficient of oxygen in the buffer solutions (1.7×10^{-5} cm^2 s^{-1}), A is the geometric area of the electrode (0.070 cm^2), C_0 is the concentration of oxygen in the solution (1.3×10^{-3} mol dm^{-3}), υ is the kinematic viscosity of the solution (0.01 cm^2 s^{-1}), and ω is the angular rotation rate of the electrode (rad s^{-1}) [42]. The linear K-L plot is an indication of the first order reaction kinetics controlled by the phenomena at the electrode surface and mass transport of oxygen species, and is used to estimate the apparent number (n) of electrons transferred during ORR at various potentials [43].

The values of n were computed from the slope of the straight lines on the K-L plots in Fig. 9. For the **Pc1/MWCNT** and **Pc2/MWCNT** catalysts, n values were calculated as 3.9 and 3.1 in the potential range of 0.7 - 0.9 V vs. Ag/AgCl. They were found considerably higher than the n values estimated as 2.5 and 2.1 for **Pc1** and **Pc2**, respectively.

Here "Fig. 9"

The previous studies [42,44] reporting the ORR catalytic behavior of CoPc compounds reveal that the ORR which is catalyzed on CoPc based-electrodes follows a 2 e^- reduction process resulting in the formation of peroxide anion. The present results suggest a possible two-step catalytic activity for the MWCNT supported CoPcs. First, a 2 e^- reduction of O_2 to HO_2 in CoPcs/MWCNT hybrid catalysts occurs, followed by disproportionation of HO_2 into OH, which enables 4 e^- reduction of O_2 in alkaline media. The n value of ~3.1 (in **Pc2/MWCNT**) was closely related to the mixed 2 e^- and 4 e^- process [45]. Nevertheless, the highest n value was calculated as 3.9 for **Pc1/MWCNT** catalyst which exhibits 4 e^- reduction of O_2. The differences in overall electron transfer number reflect the effect of the different substituents on the CoPc species catalytic mechanisms. Improved catalytic activity was indeed expected to two CoPcs including pyridine substituent, since N atoms are located in the out ring of the CoPc, thus providing additional sites for O_2 adsorption [26]. But we hypothesize that the steric hindrance and inflexibility of the hexyl substituents decreased on the one hand O_2 absorption on the N atom of pyridine group of **Pc2** on the other hand interaction between the **Pc2** and the MWCNT support. Thus **Pc2/MWCNT** showed a lower ORR activity than the **Pc1/MWCNT** hybrid catalyst.

These results show that CoPc/MWCNT hybrid catalysts including pyridine and tert(butyl) groups on the same CoPc structure have superior electrocatalytic activity compared with the previously reported CoPc/MWCNT activity data for the replacement of commercial Pt/C (n=3.97 in the alkaline media) towards the ORR [19]. However, hexa(hexyl) groups (**Pc2**) are less effective in increasing the ORR catalytic activity of the CoPc/MWCNT hybrid catalysis compared to tert(butyl) groups (**Pc1**).

4. Conclusion

In brief, we report the synthesis, characterization, electrochemical properties and ORR activity of novel cobalt phthalocyanines containing **(pyridine-4-oxy)- tri (tert-butyl)** and **(pyridine-4-oxy) - hexa (hexyl)** substituent groups. Electrochemical measurements of the compounds show that both complexes (**Pc1** and **Pc2**) have one-electron irreversible Pc(-2)/Pc(-1) and one-electron reversible CoII/CoIII couples showing the oxidation waves nearly at the same potentials in CV voltammograms. Two quasi-reversible couples are observed on the reduction side indicating metal- and ligand-centered one-electron transfers for both complexes. The SEM results demonstrate that hybrid catalysts have uniform capsule-like morphology on GCE. The change of substituent for both phthalocyanine containing one pyridine-4-oxy group considerably effect ORR catalytic activity. CoPcs/MWCNT catalysts with the influence of different substituent groups promote the desired $4e^-$ ORR in alkaline solutions while CoPcs only facilitates $2e^-$ ORR. Although all phthalocyanines and their MWCNT hybrid catalysts show a catalytic effect, tri (tert-butyl) containing CoPc/MWCNT nanocomposite exhibit excellent ORR activity at significantly less overpotential (close to 0 V) compared to hexa (hexyl) groups. ORR

activity results can be summarized as follows: **Pc1/MWCNT > Pc2/MWCNT > Pc1 > Pc2.** These impressive results can be attributed to the synergistic effect between CNT and tri (tert-butyl) group. These results demonstrating an increased ORR efficiency suggest that the materials are viable candidates for replacing existing Pt fuel cell catalysts.

Acknowledgement

This work was supported by the Scientific and Technological Research Council of Turkey (TUBITAK/TBAG 108T063).

Appendix A. Supplementary data

CCDC-863723 contains the supplementary crystallographic data for compound **2**. This data can be obtained free of charge via http://www.ccdc.cam.ac.uk/conts/retrieving.html, or from the Cambridge Crystallographic Data Centre, 12 Union Road, Cambridge CB2 1EZ, UK; fax: (+44) 1223-336-033; or e-mail: deposit@ccdc.cam.ac.uk.

References

[1] E. Yeager, J. Mol. Catal. 38 (1986) 5-25.

[2] J. Ma, Y. Liu, P. Zhang, J. Wang, Electrochem. Commun. 10 (2008) 100-102.

[3] M. Meng Li, X. Xiuxiu Ma, Y. Yanying Wu, X. Xingquan He, J Appl Electrochem. 45 (2015) 21-31.

[4] K.P. Gong, F. Du, Z.H. Xia, M. Durstock, L. Dai, Science 323 (2009) 760–764.

[5] P. Gregory, J Porphyr. Phthalocyanines 4 (2000) 432-437.

[6] J. Li, J.S. Lindsey, J. Org. Chem. 64 (1999) H9101-9108.

[7] H.S. Zhou, I. Honma, AdV. Mater. 11 (1999) 683-685.

[8] M. Hanack, T. Schneider, M. Barthel, J.S. Shirk, S.R. Flom, R.G.S. Pong, Coord. Chem. ReV. 219-221 (2001) 235-258.

[9] T. Ceyhan, A. Altındal, M. K.Erbil, Ö. Bekaroglu Polyhedron 25 (2006) 737-746.

[10] T. Goslinski, T. Osmalek, K. Konopka, M. Wierzchowski, P. Fita, J. Mielcarek, Polyhedron 30 (2011) 1538-1546.

[11] Z.P. Li, B.H. Liu, J Appl Electrochem 40 (2010) 475-483.

[12] L.N. Ramavathu, K.K. Maniam, K. Gopalram, R. Chetty, J Appl Electrochem 42 (2012) 945-95.

[13] R. Jasinski, Nature 201 (1964) 1212−1213.

[14] E. Song, C.N. Shi, F.C. Anson, Langmuir 14 (1998) 4315-4321.

[15] J. Zagal, M. Pa´ez, A.A. Tanaka, J.R. dos Santos Jr., C.A. Linkous, J Electroanal. Chem. 339 (1992) 13-30.

[16] S. Iijima, Nature 354 (1991) 56-58.

[17] R.H. Baughman, A.A. Zakhidov, W.A. Heer, Science 297 (2002) 787-792.

[18] Y.P. Sun, K.F. Fu, Y. Lin, W.J. Huang, Acc. Chem. Res. 35 (2002) 1096-1104.

[19] A. Morozan, S. Campidelli, A. Filoramo, B. Jousselme, S. Palacin, Carbon 49 (2011) 4839-4847.

[20] Z. Xu, H. Li, G. Cao, Q. Zhang, K. Li, X. Zhao, J. Mol. Catal. A Chem. 335 (2011) 89-96.

[21] H.J. Li, Z.W. Xu, K.Z. Li, X.H. Hou, G.X. Cao, Q.L. Zhang, Z.Y. Cao, J. Mater. Chem. 21 (2011) 1181-1186.

[22] G.F. Xu, Z.F. Li, S.W. Wang, X.J. Yu, J. Power Sources 195 (2010) 4731-4735.

[23] V. Mani, R. Devasenathipathy, S.M. Chen, J.A. Gu, S.T. Huang, Renewable Energy 74 (2015) 867-874.

[24] M. Xu, C. Li, H. Ren, L. Ding, K. Xu, J. Geng, J. Mol. Catal. A Chem. 390 (2014) 69-75.

[25] J. Qiaoa, B. Tianc, L. Xua, Y. Liub, P. Xua, J. Shia, S. Liuc, Electrochimica Acta 96 (2013) 298-305.

[26] L. Cui, G. Lv, X. He, J. Power Sources 282 (2015) 9-18.

[27] R. Baker, D.P. Wilkinson, J. J. Zhang, Electrochimica Acta 54 (2009) 3098-3102.

[28] S. Matsudaa, S. Moribi, Y. Kuboc, K. Uosakic, K. Hashimotoa, S. Nakanishia, Chem. Phys. Lett. 620 (2015) 78-81.

[29] S. Khene, T. Nyokong, Electroanalysis 23 (2011) 1901-1911.

[30] Bruker, SADABS, Bruker AXS Inc., Madison, Wisconsin, USA, 2005.

[31] Bruker APEX2 (Version 2011.4-1). Bruker AXS Inc., Madison, Wisconsin, USA, 2008.

[32] G.M. Sheldrick, Acta Crystallogr., Sect. A 64 (2008) 112-122.

[33] A.L. Spek, Acta Crystallogr., Sect. D 65 (2009) 148-155.

[34] C.F. Macrae, I.J. Bruno, J.A. Chisholm, P.R. Edgington, P. McCabe, E. Pidcock, L. Rodriguez-Monge, R. Taylor, J. van de Streek, P.A. Wood, J. Appl. Crystallogr. 41 (2008) 466-470.

[35] K. Brandenburg, DIAMOND 3.1 for Windows. Crystal Impact GbR, Bonn, Germany, 2006.

[36] H.T.S. Britton, R.A. Robinson, J. Chem. Soc. 0 (1931) 1456-1462.

[37] M. Hanack, P. Haisch, H. Lehmann, L.R. Subramanian, Synthesis 4 (1993) 387-390.

[38] H. Li, T.J. Jensen, F.R. Fronczek, M.G. Vicente, J.Med.Chem. 51 (2008) 502-511.

[39] D.J. Scott, M.J. Fuchter, A. E. Ashley, Angew. Chem. Int. Edit. 53 (2014) 10218-10222.

[40] B. Agboola, K. I. Ozoemena, T. Nyokong, Electrochimica Acta 51 (2006) 4379-4387.

[41] K. Elouarzaki, R. Haddad, M. Holzinger, A. Le Goff, J. Thery, S. Cosnier, J. Power Sources 255 (2014) 24-28.

[42] T.T. Tasso, T. Furuyama, N. Kobayashi, Inorg. Chem. 52 (2013) 9206-9215.

[43] Z. Ou, A. Lu, D. Meng, S. Huang, Y. Fang, G. Lu, K.M. Kadish, Inorg. Chem. 51 (2012) 8890-8896.

[44] R. Chen, H. Li, D. Chu, G. Wang, J. Phys. Chem. C 113 (2009) 20689-20697.

[45] K. Shigehara, F.C. Anson, J. Phys. Chem. 86 (1982) 2776-2783.

Figure Captions

Fig. 1 Crystal structures of compound **2** with the atom-numbering scheme. Displacement ellipsoids are drawn at the 50% probability level. The hydrogen atoms have been omitted for clarity. *Symmetry* code (#): -x+2, y, -z+3/2.

Fig. 2 Cyclic voltammograms of 5.0×10^{-4} mol/l **Pc1** and **Pc2** in TBAP/THF solvent system versus Ag/AgCl (scan rate 0.05 Vs^{-1}).

Fig. 3 CVs of (a) **Pc1** and (b) **Pc2** in TBAP/THF solution. Scan rates (Vs^{-1}): 0.05, 0.1, 0.2, 0.3, 0.4, 0.5.

Fig. 4 Ip_a vs. square root of scan rate for the four processes (labelled **I**, **II**, **III** and **IV**) for (a) **Pc1** and (b) **Pc2**.

Fig. 5 SEM images of (a) **Pc1** and (b) **Pc1/MWCNT**, (c) **Pc2/MWCNT** composites.

Fig. 6 Reduction of oxygen on (a) **Pc1** and **Pc1/MWCNT**, (b) **Pc2** and **Pc2/MWCNT** on GC electrode in alkaline media (pH 11.8). Scan rate: 100 mV/s.

Fig. 7 Reduction of oxygen on (a) **Pc1** and **Pc1/MWCNT**, (b) **Pc2** and **Pc2/MWCNT** on GC electrode in acidic media (pH 2.4). Scan rate: 100 mV/s.

Fig. 8 Polarization curves in air saturated buffer solutions (pH 11.8). Coated with (a) **Pc1**, (b) **Pc1/MWCNT**, (c) **Pc2**, (d) **Pc2/MWCNT and** (e) **bare electrode** (scan rate: 0.05 V/s).

Fig. 9 Levich−Koutecky plots at different potentials coated with (a) **Pc1**, (b) **Pc1/MWCNT**, (c) **Pc2**, (d) **Pc2/MWCNT** and (e) uncoated **GC** rotating electrode vs. Ag/AgCl.

Scheme Captions

Scheme 1 Synthesis of **Pc1** and **Pc2** (i) metal salt, DMAE, reflux.

Compound	2
Empirical formula	$C_{18}H_{28}Br_2$
Formula weight	404.22
Temperature (K)	120(2)
Crystal system	Monoclinic
Space group	*C2/c*
a (Å)	10.15650(10)
b (Å)	9.48860(10)
c (Å)	18.7689(2)
β (°)	98.7280(10)
Volume ($Å^3$)	1787.83(3)
Z	4
Density (calc, Mg/m^3)	1.502
Absorption coeff. (mm^{-1})	4.525
F(000)	824
θ_{max} (°)	25.12

Reflections collected	6847
Independent reflections	1596
R_{int} (merging R value)	0.0177
Parameters	92
R ($F^2>2\sigma F^2$)	0.014
wR (all data)	0.039
Goodness-of-fit on F^2	1.067

Table 1 X-ray crystallographic data and refinement parameters for compound **2**.

Complex	**Couple**	**υ (mV/s)**	**E_{pa} (V)**	**E_{pc} (V)**	**ΔE_p (mV)**	**$E_{1/2}$ (V)**	**I_{pa}/I_{pc}**
Pc1	I	50	-1.35	-1.54	190	-1.45	1.18
	II		-0.31	-0.45	140	-0.38	1.23
	III		0.79	0.73	60	0.77	0.80
	IV		1.13	1.00	130	1.07	2.55
	I	500	-1.33	-1.58	250	1.46	1.26
	II		-0.27	-0.5	230	0.39	1.23
	III		0.78	0,7	80	0.74	1.01
	IV		1.10	1.01	90	1.06	0.32
Pc2	I	50	-1.40	-1,48	80	-1.44	1.17
	II		-0.33	-0.45	120	-0.39	1.02

III		0.75	0.69	60	0.72	0.95
IV		1.12	0.98	140	1,05	0.85
I	500	-1.38	-1.52	140	-1.45	1.21
II		-0.30	-0.50	200	-0.34	1.15
III		0.76	0.67	90	0.72	1.01
IV		1.13	0.95	180	1.04	1.36

Table 2 Electrochemical Parameters of $5.0x10^{-4}$ M CoPc complexes in THF/ TBAP at 50 and 500 mV/s scan rates.

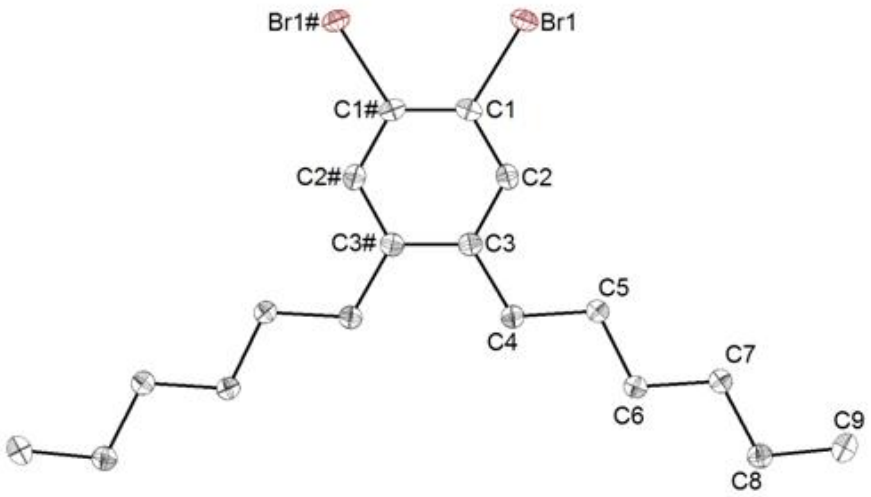

Fig. 1.

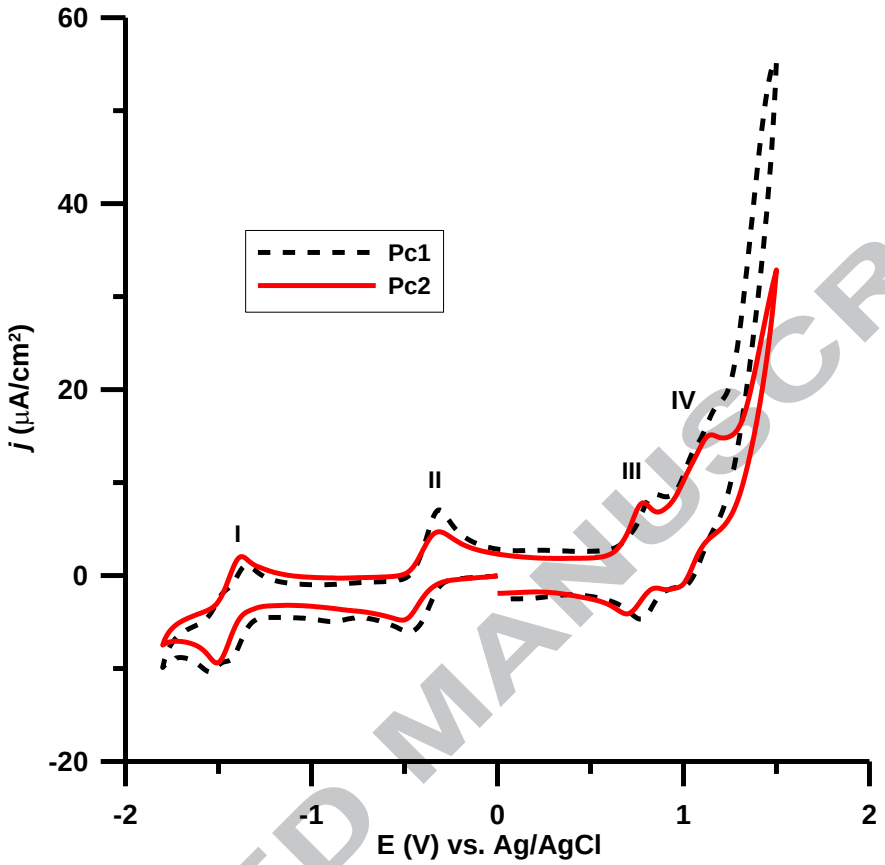

Fig. 2.

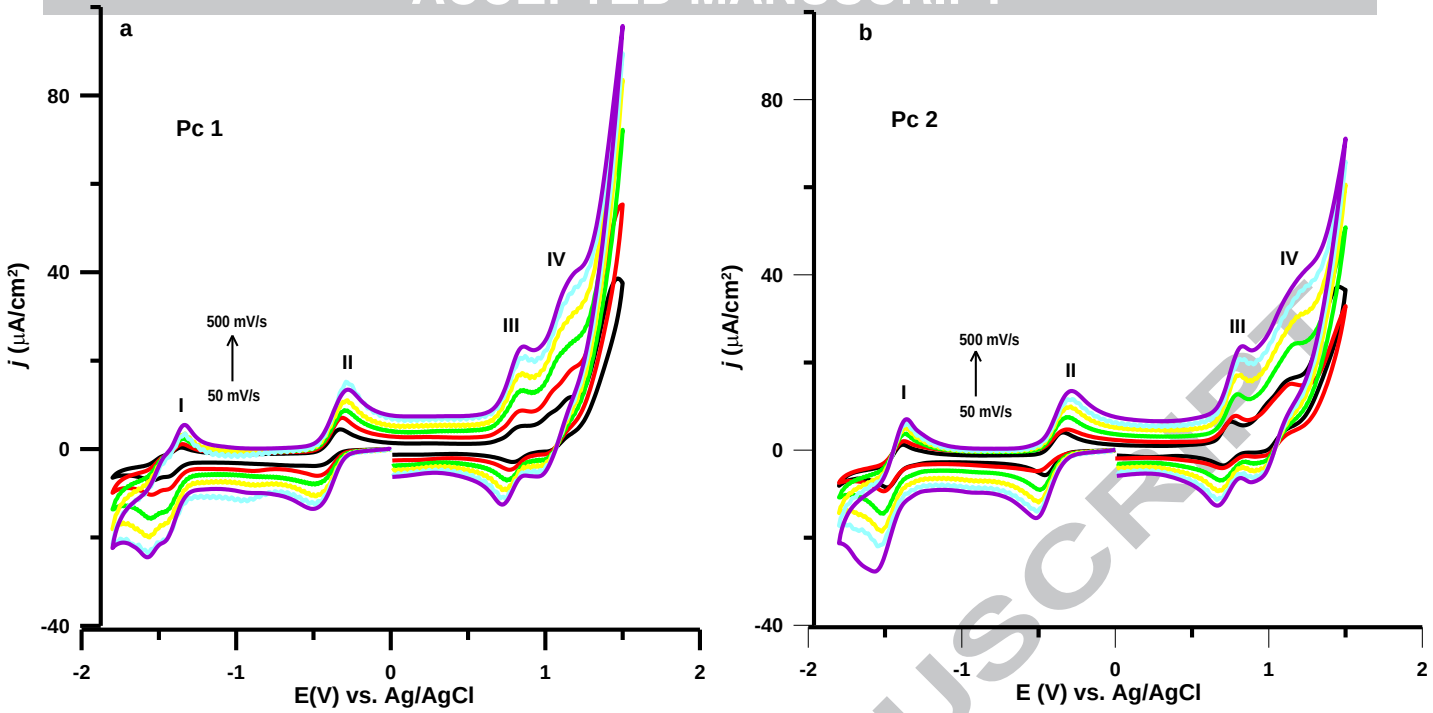

Fig. 3.

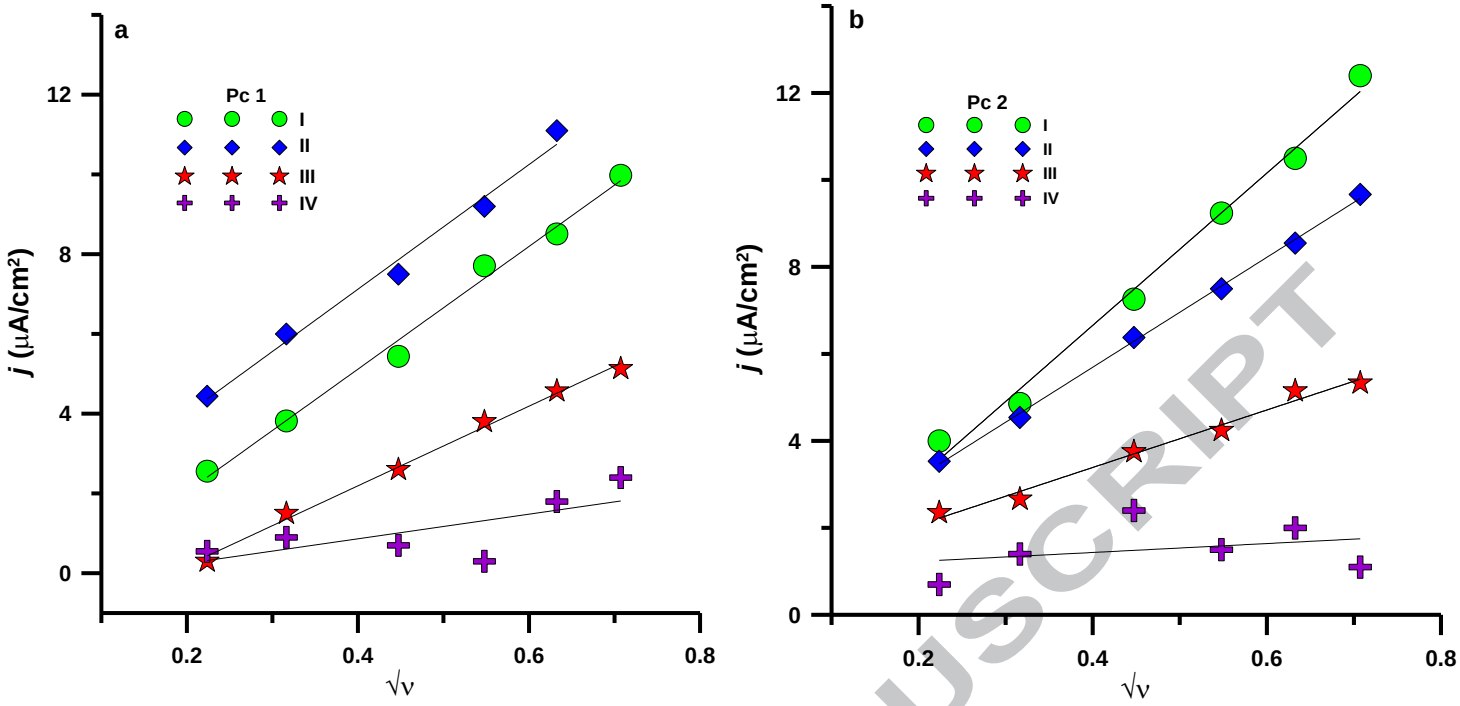

Fig. 4.

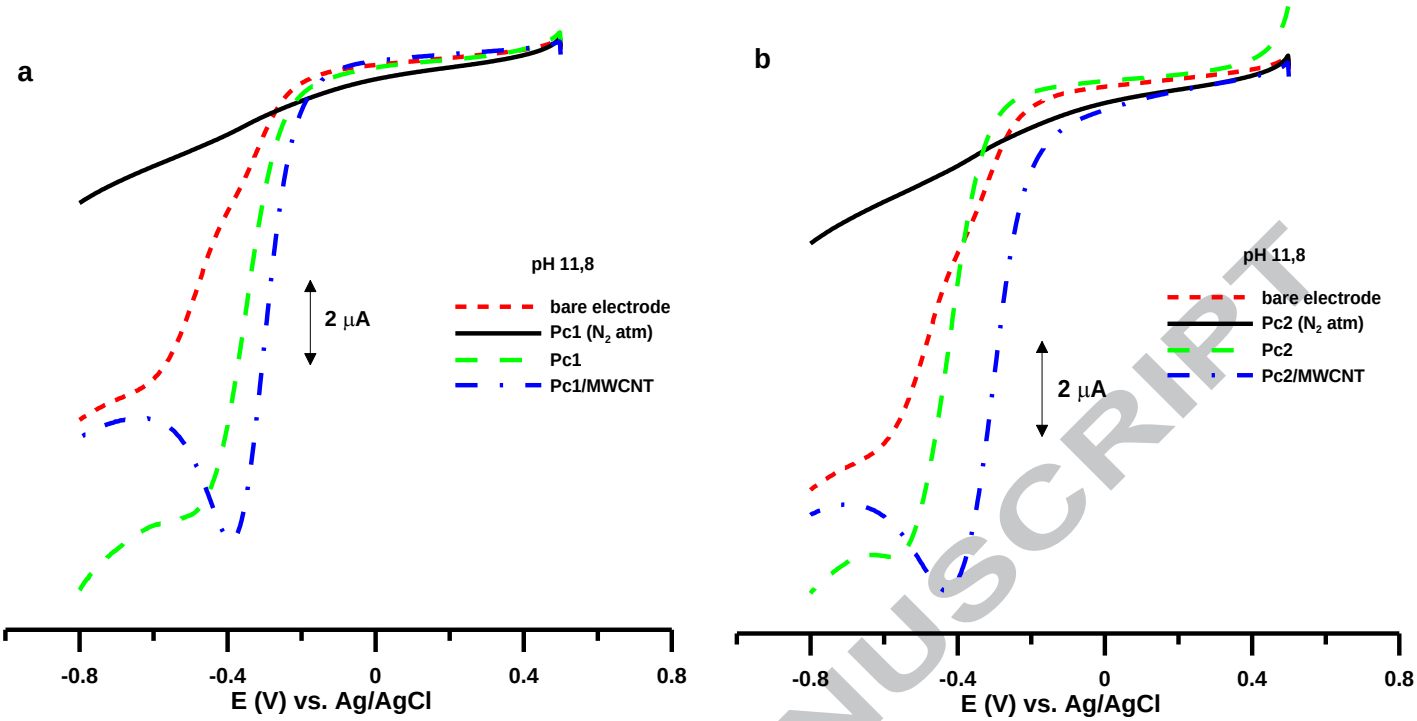

Fig. 6.

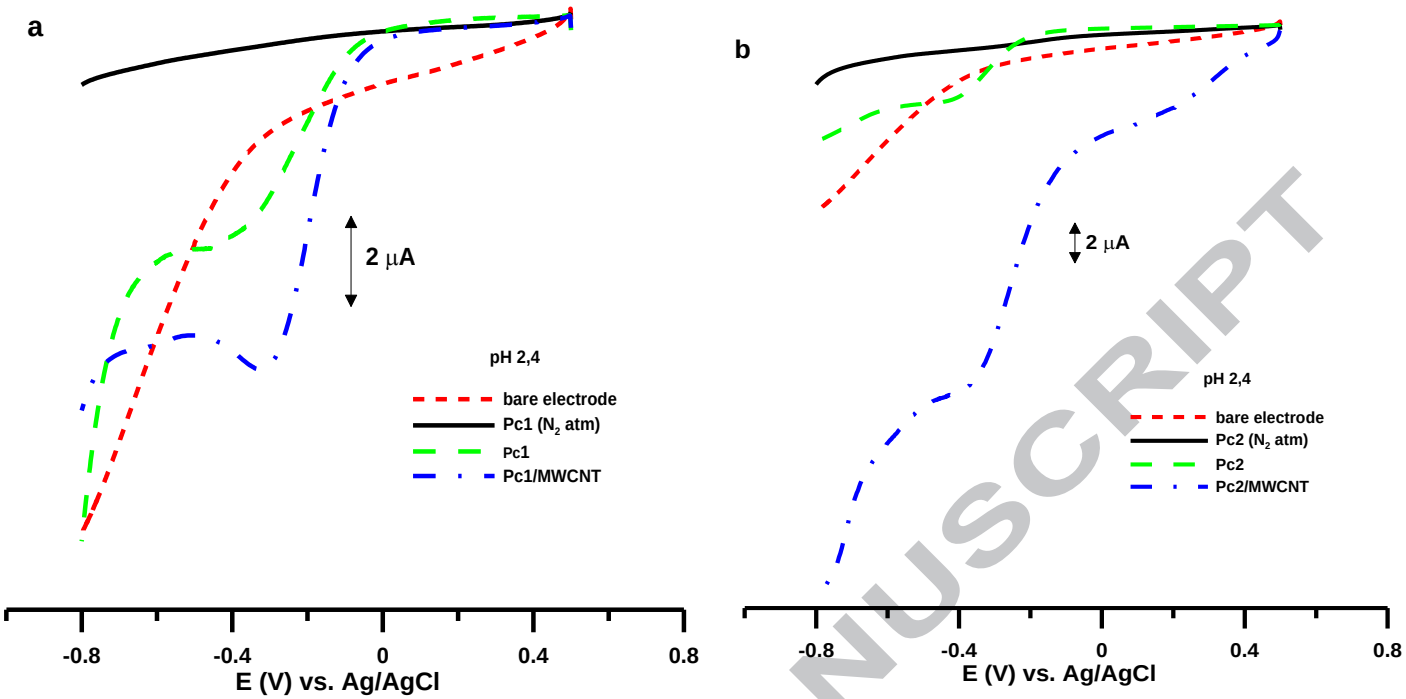

Fig. 7.

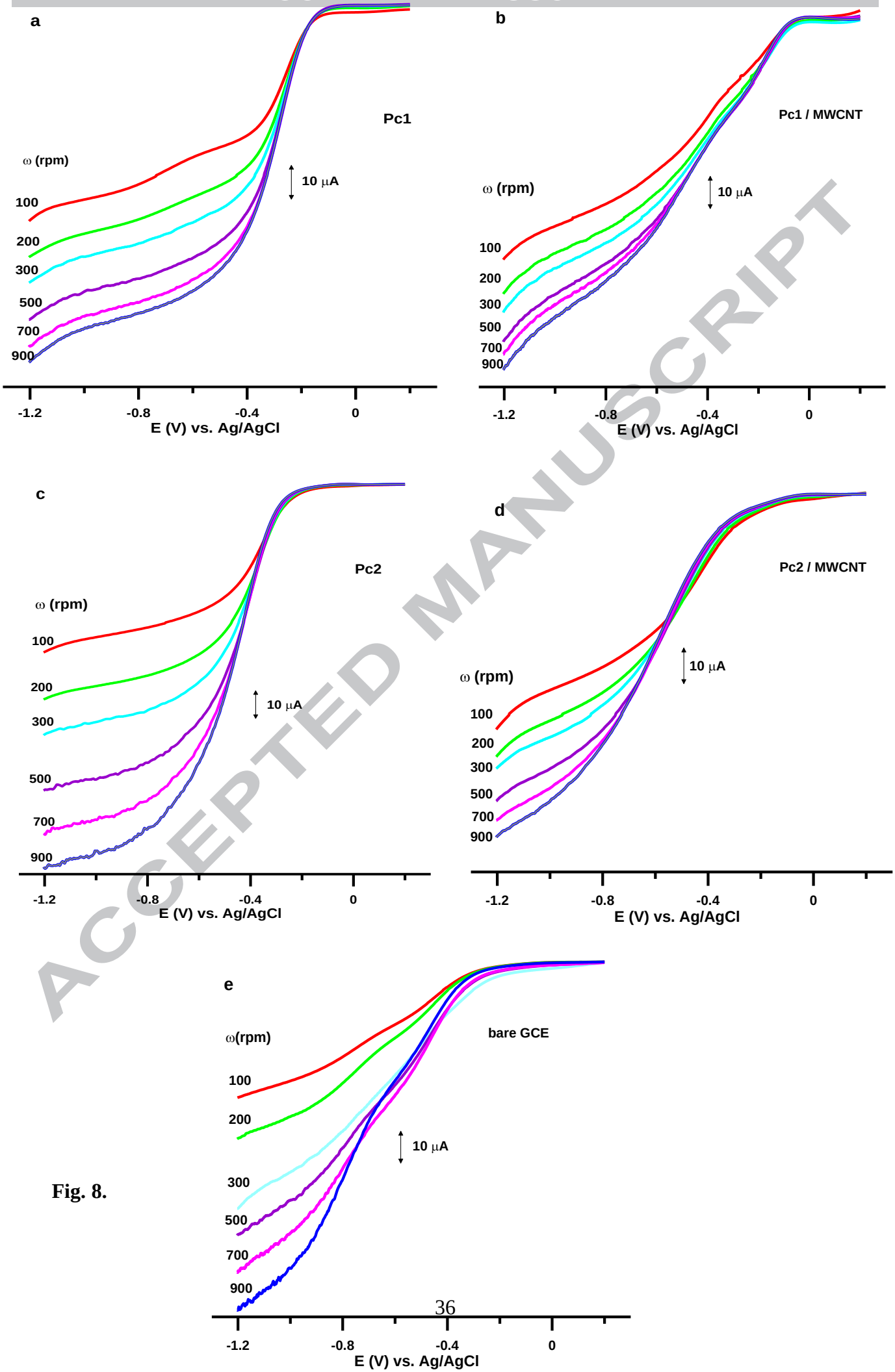

Fig. 8.

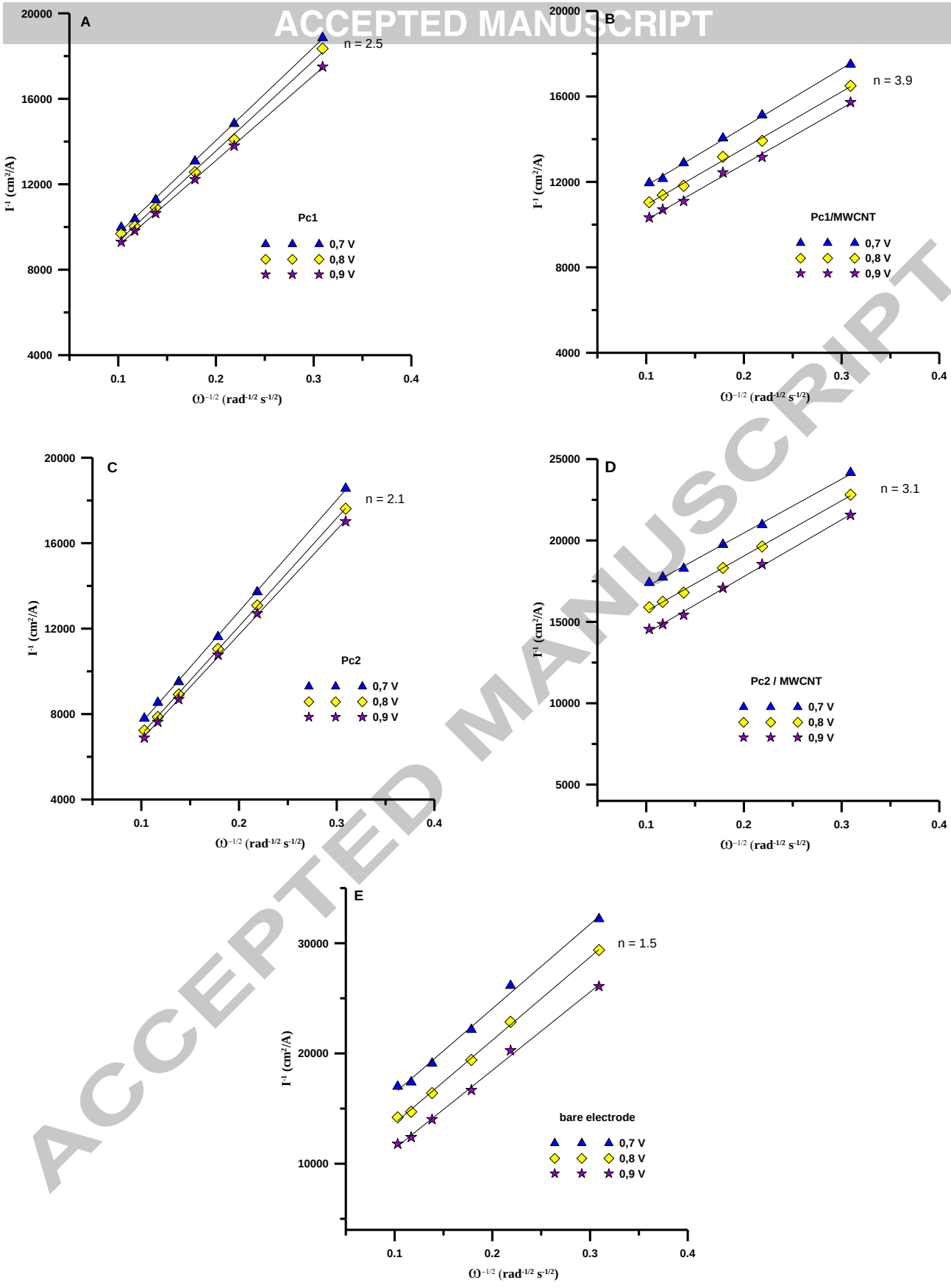

Fig. 9.

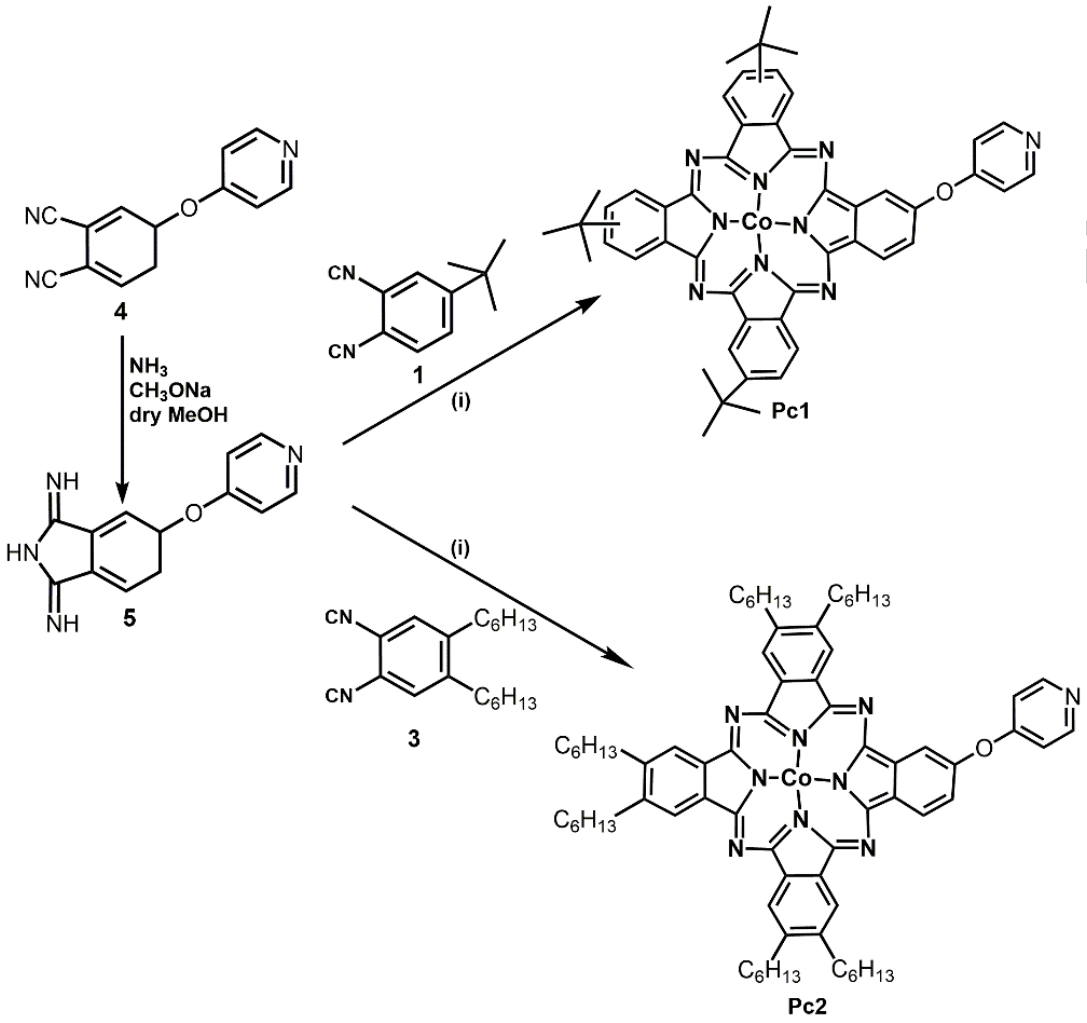

Scheme 1

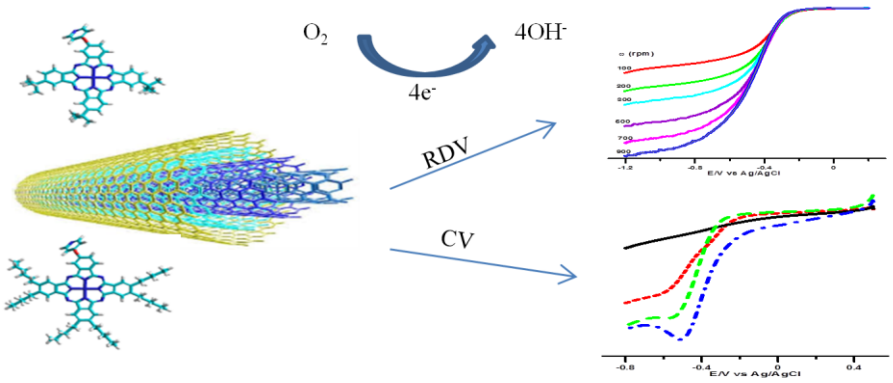

Synopsis

Two novel Co phthalocyanine complexes were synthesized and structurally characterized. The effect of substituents on ORR electrocatalytic activities of CoPc complexes and CoPc/MWCNT hybrid catalyst were investigated in alkaline and acidic media. CoPcs/MWCNT nanocomposites exhibited excellent ORR activity with the desired 4e- ORR in alkaline solutions. This behaviors make them potential candidates for fuel cell.